Light Metals 2014
Edited by: John Grandfield
TMS (The Minerals, Metals & Materials Society), 2014

The Near-Rapid Solidification Behavior of AA1070 Aluminum Alloy

Y. L. Liu, L. Zhang, Y. H. Zhao, J. J. Wang, C. Z. Liu
Shenyang Aerospace University, Shenyang, China

Keywords: aluminum alloy, near-rapid solidification, continuous strip casting

Abstract

Continuous strip casting process creates a near-rapid cooling condition. In this paper, the solidification behaviors of AA1070 alloy under near-rapid cooling condition have been investigated using the metallographic-EDX method. Although the AA1070 is a commercial pure aluminum alloy with limited amount of iron and silicon, its solidification behavior is quite complicated under the condition of near rapid solidification. When the alloy solidified under the condition of equilibrium or near-equilibrium solidification, the elements of iron and silicon segregated to the final solidification zone and formed coarse phases at the grain boundaries. With the increase in cooling rate to near-rapid cooling, some fine eutectic structures appeared at grain boundaries and inter-dentrites. Both binary eutectic of α-Al+Al_tFe and ternary eutectic of α-Al+Al_tFe(Si)+Al_mFe(Si) were observed.

Introduction

Near-rapid solidification is usually referred to as the solidification process with cooling rate between 10^0—10^3 K/s[1,2]. For example, the solidification of alloy in continuous strip casting process is a near-rapid solidification. The casting rolls or belts create a strong cooling, which gives the castings a high solidification rate; much higher than that of the normal casting process. Continuous strip casting, as a short process technology, has been receiving more and more attention from aluminum industries. More and more aluminum alloy foils and sheets, even some plates, are produced via this process[3]. Although the cooling rate in continuous strip cast is not high enough to classify the process as rapid solidification, it was found that the as-cast microstructures of the continuous strip cast slabs or bars are quite different from that of direct chill casting process, even in the commercial pure aluminum, such as AA1070 alloy which is a common alloy used in continuous strip caster. It is interesting to investigate the solidification process under near-rapid cooling.

AA1070 alloy is commercial pure aluminum alloy. Its chemical composition is very simple with low iron and low silicon. But its microstructure is not simple. Although the contents of iron and silicon in this alloy are quite low, almost all the iron forms intermetallic secondary phases since the solid solubility of iron in aluminum is less than 0.05 % at equilibrium. According to the Al-Fe-Si ternary equilibrium diagram [4], aluminum with low iron and silicon contents should contain primary α-Al and intermetallic phases of an Al_3Fe, Al_8Fe_2Si and Al_5FeSi type. Through both laboratory and industrial examinations, a large number of iron-containing intermetallic phases have been identified in the unalloyed aluminum in as-cast state, depending on the solidification conditions and alloy composition[5-12]. These intermetallics influence the material properties of the material during subsequent fabrication steps and play a crucial role for the material quality[13]. It has been observed that among them, the needlelike Al_3Fe and β-AlFeSi phases are deleterious to the mechanical properties. Thus, it is of considerable technological interest to control the morphology and distribution of these phases in order to eliminate the negative effects.

Despite several decades of experimental examinations and theoretical efforts, the details of the formation of binary and ternary iron-containing intermetallics in solidifying Al alloys have not been fully understood. Especially, the solidification behavior of the aluminum alloys under the condition of near-rapid cooling is lack of investigation. Near-rapid solidification is a transition zone between near-equilibrium solidification and rapid solidification. In this transition zone, the solute-redistribution, solidification structure and the stability of solidification interface are much different from that of near-equilibrium solidification[2]. Although AA1070 alloy is a simple aluminum alloy, it is assumed that under the condition of near-rapid cooling, its as-cast microstructures are quite complicated. This work is to investigate the influence of cooling rate on the as-cast microstructure of the AA1070 aluminum alloy.

Experimental Procedures

The samples used for this study were cut out from a bar with a section of about 50 X 60 mm, which was cast by wheel-belt continuous casting machine and used for the production of aluminum rod. The chemical composition of the bar was determined by means of Emission Spectrography Analyzer and is provided in Table 1. The cut samples with a size of approximately 25X25X40 mm were remelted in an alumina ceramic crucible in an air furnace by heating the material to 750°C. The samples were kept for at least10 minutes at the aforementioned temperature, in order to melt the materials entirely and to homogenize the composition. The molten materials were then solidified under the different conditions listed below.

Sample 1: solidified in a ceramic crucible in furnace. After reaching the intended temperature, the furnace was turned off and the sample was cooled down with the cooling of furnace. The average cooling rate before the start of solidification was approximately 0.037°C/s.

Sample 2: solidified in a refractory backed ceramic crucible in air. One smaller crucible was placed in a larger ceramic crucible. The gap between the two crucibles was filled with refractory powders. The larger crucible was covered by a lid. After reaching the intended temperature, the crucible backed with the larger crucible and refractory powders was moved out of the furnace and placed on floor. The sample was cooled down and solidified. The average cooling rate before the start of solidification was approximately 0.45°C/s.

Sample 3: solidified in a ceramic crucible in air. After reaching the intended temperature, the crucible was moved out of the furnace and the sample was cooled down and solidified in air. The average cooling rate before the start of solidification was approximately 1.63°C/s.

Table 1 Chemical Composition of Alloy Examined (Emission Spectrography Analysis), wt%

Fe	Si	Ni	Ti	V	Mn	Zn	Cu	B	Cr	Zr	Al
0.12	0.056	0.002	0.001	0.005	0.003	0.014	0.005	0.019	0.002	0.002	Bal.

Sample 4: solidified in a thin iron mould at room temperature (inner diameter 30 mm; outer diameter 40 mm, height 50 cm). The average cooling rate before the start of solidification was approximately 9.6°C/s.

Sample 5: solidified in a thick iron mould at room temperature (inner diameter 25 mm; outer diameter 70 mm, height 50 cm). The average cooling rate before the start of solidification was approximately 34.5°C/s.

Sample 6: solidified in a double-side water cooled iron mould at room temperature. The casting size was 60 X 40 X10 mm. Cold water was continuously injected to the two side walls. The average cooling rate before the start of solidification was approximately 64.7°C/s.

In these experiments, the temperature was measured by using a K-type thermocouples. The thermocouple was inserted along the centerline of the crucible or model halfway into the melt. An evolution of temperature with time was recorded every 0.1 second. The acquired temperature-time dependencies were numerically differentiated to catch thermal effects accompanying solidification and evaluate the cooling rates achieved at different solidification modes. These estimations are provided following the sample definition above. The cooling rates of samples 3 to 6 were in the range of near-rapid.

Samples for metallographic investigations were cut out from the alloy in the vicinity of the thermocouple's tip, ground with SiC papers, polished with 3 μm alumina water solution and finally polished using diamond solutions. The samples were etched with a reagent (25 vol.% HNO_3 + 2 vol.% HF + 73 vol.% H_2O) and the microstructures of the samples were examined using an OLYMPUS GX71 optical microscope. A Zeiss scanning electron microscopy with OXFORD energy dispersive X-ray (EDX) analyzer was employed to identify intermetallic compounds.

Results

Solidification Behavior under Slow Cooling

Figure 1 shows the cooling curve of the alloy during solidification in furnace. From the time-temperature curve, it was calculated that the average cooling rates were 0.037°C/s before the start of the solidification process and 0.028°C/s after solidification was completed, by using the formula dT/dt, and was computed from the approximate straight line portion of the cooling curve. The cooling rate dramatically changed between the two points. At about 658 °C, the cooling rate dropped to close to zero, which was associated with the valley (a) and then vacillated at this level. This drop in cooling rate corresponded to the start of the solidification and the formation of the primary α-Al dendrites. The release of the solidification latent heat prevents the material from cooling further, which made the thermal arrest last about 1,580 seconds. Then, the cooling rate increased again. This corresponded to the finish of the releasing of the latent heat. The second thermal event occurred at about 643°C, associated with the valley (b), and third thermal event occurred at about 632°C, associated with the valley (c). These two events lasted only a very short amount of time. It was assumed that only a small amount of phases formed in these two thermal events. Then, the cooling rate of the material reduced gradually before finally reaching the cooling rate of the furnace, after which, the alloy cooled at the same rate of the cooling rate of the furnace.

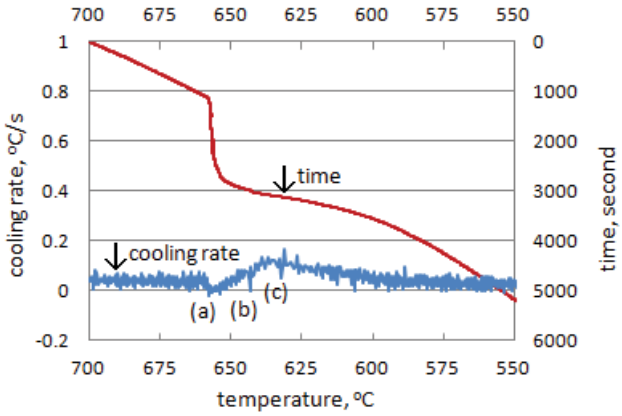

Fig. 1 the cooling curve of the Sample 1

The typical as-cast microstructure of the Sample 1 solidified in a furnace at a cooling rate of 0.037°C/s is shown in Figure 2(a). It consists of primary α-Al dendrites and some eutectic phases. The eutectic phases are mainly Al-Fe and AlFe(Si) phases located at the grain boundaries. At the triangle grain boundaries, most of the eutectics displayed typical eutectic structures, which appeared as lamellar or Chinese-script structure. Some eutectic structures formed a dotted-line type structure and arranged along the grain boundaries. In addition, some long strip-like structures were also observed, as shown in Figure 2(b).

A routine method for identifying the intermetallics is to measure the composition of the intermetallics and estimate their Fe/Si atomic ratios using EDX. The results of the EDX examination are summarized in Table 2. The results indicated that the strip-like phase is Al-Fe intermetallic with a relatively low content of iron (less than10%). According to literature [6], it should be Al_tFe. The phases located at the grain boundaries are also Al-Fe intermetallics, but they contain much higher composition of iron. Although they are of different morphologies, the EDX analysis confirmed that they possess roughly the same compositions, as listed in Table 2. It is assumed that they are Al_3Fe with a small amount of Si. The content of silicon in the alloy is 0.056wt%, but no significant content of silicon in the eutectic phases was detected. In addition, in all measurements, small amount of nickel was detected, see Table 2. The content of nickel in the alloy is very low (0.002wt%), it segregated into the final solidification zone and was trapped in the eutectic compounds.

Table 2 the EDX results of the eutectic compounds

spot	Fe, wt%	Si, wt%	Ni, wt%	Al, wt%
Strip-like 1	8.0	0	0.3	91.7
Strip-like 2	8.3	0	0.4	91.3
Lamellar 1	34.2	0.7	1.3	63.8
Lamellar 2	32.9	0.8	2.8	63.5

Lamellar 3	29.5	0.7	1.0	68.9

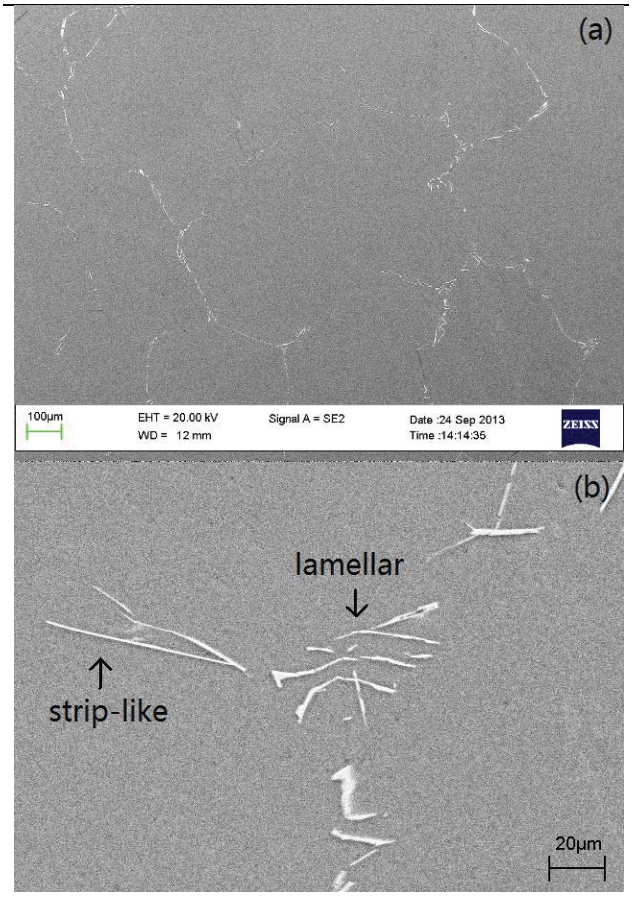

Fig. 2 (a) as-cast microstructures of Sample 1 and (b) strip-like and lamellar structures

It can be seen by linking the microstructures with the thermal analysis that valley (a) was corresponded to the formation of primary phase. The formation of the Al_tFe intermetallic was associated with the valley (b) and Al_3Fe phase associated with valley (c). It was assumed that two eutectic reactions occurred in the final solidification zone. At around 643°C, eutectic reaction L→ α-Al + Al_tFe occurred. But the eutectic phase Al_tFe devoiced at the grain boundaries and formed sheet-like structure and displayed a strip-like structure on the metallographic face. The eutectic reaction L→ α-Al + Al_3Fe occurred at around 632°C which ended the solidification process.

Solidification Behavior under Near-Rapid Cooling

Table 3 lists some characteristics of the cooling curves. The thermal events in solidification were a function of the cooling rate. With the increase in cooling rate, the solidification temperature of the alloy deceased and the thermal arrest time during solidification shortened, which reflected shortening of the solidification time. All cooling rate curves show first valley (primary α-Al) and second valley (eutectic reaction), but no third valley was shown in the samples solidified under near-rapid cooling, as shown in Figure 3. This means that in the sample solidified at a higher cooling rate, the second eutectic reaction was suppressed or too small to create a valley on the cooling curve. Increasing cooling rate gave rise to the creation of supercooling. microstructures. When the material solidified at a cooling rate of

In Sample 4 solidified at 2.7°C/s, a supercooling of 0.2°C was detected. It increased to 7.8°C in Sample 6, which solidified at 64.7°C/s, see Figure 4. Under the condition of slow cooling, the cooling rates of the metal were roughly the same before and after solidification. However there was a great difference in cooling rate before and after solidification under the near-rapid solidification. For example, Sample 5 was cooled at 34.5°C/s before solidification and only 9.8°C/s after solidification. Increasing the cooling ability of the model would not increase the cooling rate of the metal after solidification. In Sample 6, the cooling rate before solidification was increased to as high as 65°C/s , the cooling rate after solidification was still only 10.3°C/s, not much increase was achieved. This was attributed to the difference in heat transfer in liquid (before solidification) and solid (after solidification). It is assumed that increasing the cooling strength of the model could increase the cooling rate of metal before solidification, but could not remarkably increase the cooling rate after solidification.

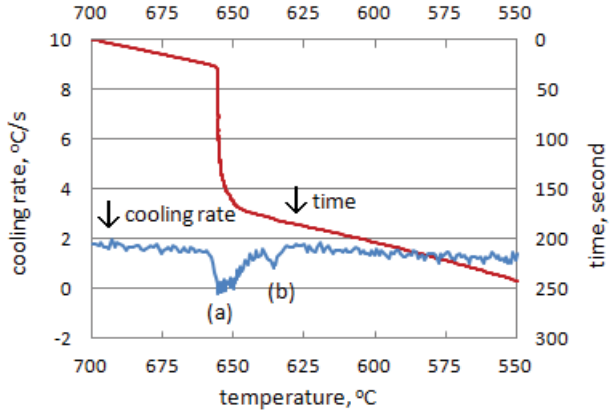

Fig. 3 the cooling curve of Sample 3

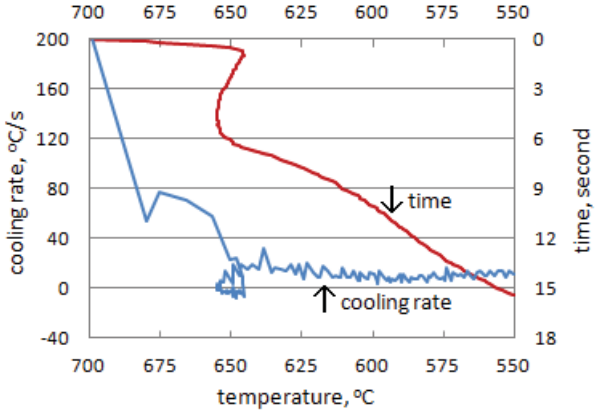

Fig. 4 the cooling curve of Sample 6

With the increase in cooling rate, the microstructure changed. The eutectic clusters reduced in size and the strip-like phase reduced both in number and size. In Sample 2 which solidified at a cooling rate of 0.45°C/s, the eutectic structure still displayed lamellar of Chinese script morphologies, but was smaller in size compared to Sample 1. In addition, the amount of the strip-like phase was less.

Figures 5 to 7 shows the as-cast microstructures of the alloy solidified at near-rapid cooling rates. When cooling rate increased to near-rapid cooling, significant change occurred in the as-cast 1.63°C/s, although the solidification structures still consist of

Table 3 some characteristics of the cooling curves

Sample	Thermal arrest time, s	Solidification temperature, ^oC	Average cooling rate (700—550^oC), $^oC/s$	Cooling rate before solidification, $^oC/s$	Cooling rate after solidification, $^oC/s$	Supercooling. ^oC
Sample 1	1580	658	0.029	0.037	0.028	0
Sample 2	332	656	0.30	0.452	0.358	0
Sample 3	134	656	0.62	1.63	1.26	0
Sample 4	23	654	2.7	9.6	3.7	0.2
Sample 5	7.4	653	7.3	34.5	9.5	0.6
Sample 6	4.9	645	9.8	64.7	10.6	7.8

primary aluminum dendrites and some eutectic intermetallic phases, it can be seen that the eutectic intermetallic phases displayed a different structure. Only very few strip-like phases were observed and their sizes were very small. At triangle grain boundaries, unlike the coarse triangle cluster of eutectics formed at slow cooling, the eutectic cluster rounded up, see Figure 5(a). These eutectic compounds were fine and still appeared as lamellar or Chinese-script structure. In addition, some fine button-like eutectic clusters appeared in round shape or irregular form and were isolated at grain boundaries and inter-dentrites. At high magnification, it can be seen that there existed two types of eutectic structures: one was typical lamellar or Chinese script type eutectics; the other consisted of typical lamellar or Chinese script type eutectics plus particle-like phase, see Figure 5(b) and (c).

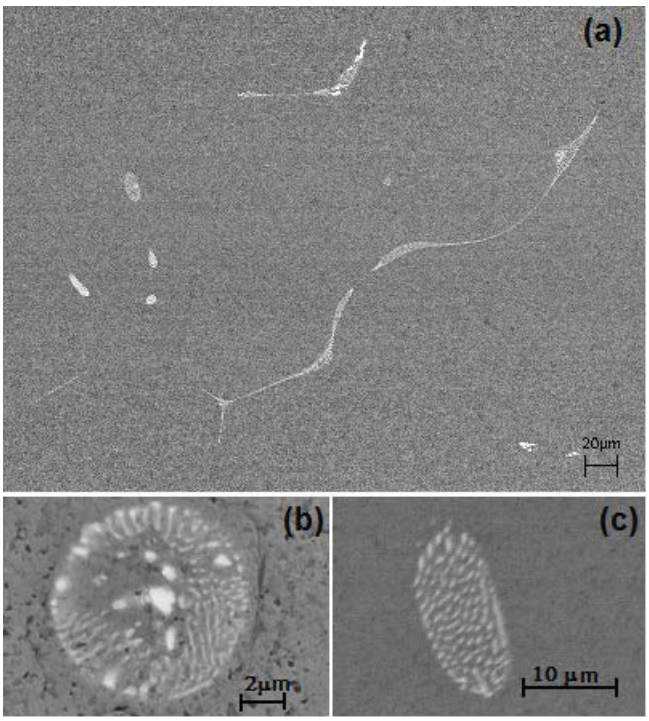

Figure5 (a) as-cast microstructures of Sample 3,
(b) lamellar plus particle-like structure and
(c) short rod or lamellar structures

EDX analysis on the fine eutectic clusters, as shown in Figure 5, indicated that the lamellar or Chinese script type eutectics phases were Al-Fe intermetallics, but the content of iron is quite low, similar to the composition of Al_tFe in Sample 1. The coarse particles-like phases are of higher iron content and contain small amounts of silicon, see Table 4. It is assumed that the lamellar or Chinese script type eutectics phases and the particle-like phases are different intermetallics. The lamellar or Chinese script phase is also Al_tFe type, but contain small amount of silicon ($Al_tFe(Si)$); the particle-like phase is $Al_mFe(Si)$. It is assumed that other than the binary eutectic reaction $L \rightarrow \alpha\text{-}Al + Al_tFe(Si)$, ternary eutectic reaction $L \rightarrow \alpha\text{-}Al + Al_tFe(Si) + Al_mFe(Si)$ took place in some final solidification zones.

Table 4 the EDX results of the eutectic compounds

Spot	Fe, wt%	Si, wt%	Ni, wt%	Al, wt%
Coarse particle	17.1	0.6	0	82.3
Lamellar 1	8.5	0	0	91.5
Lamellar 2	9.3	1.2	0	89.5
Short rod	8.0	0.9	0	91.1

Comparing Samples 3, 4 and 5, it was found that with further increase in cooling rate, the triangle-type eutectic structure at the triangle grain boundaries reduced gradually; the number of the fine button-like eutectic structure at grain boundaries and inter-dendrites increased. Sample 4 solidified at a cooling rate of 9.6$^oC/s$, the triangle-type eutectic structures at triangle grain boundaries were much less; the fine button-like eutectic clusters increased in number and decreased in size. In Sample 5 solidified at a cooling rate of 34.5$^oC/s$, the triangle-type eutectic clusters at triangle grain boundaries almost fully disappeared; the fine button-like eutectic clusters increased in number and decreased in size to a further extent, see Figure 6. However no significant change occurred in their chemistry composition. The EDX analysis indicated that the short-rods or small particles phase are of similar chemistry as the lamellar or Chinese script type eutectics phases.

In Sample 6, which solidified at a cooling rate of 64.7$^oC/s$, new phenomenon appeared. The eutectic clusters were much less in number and smaller in size than that in Sample 5. The morphology of the eutectic compounds was also different. They displayed flake-like structures, instead of lamellar as shown in previous Samples, see Figure7. From the EDX analysis, it was found that the eutectic phases were also Al_tFe.

Discussion

During solidification, with the growth of α-Al grains, the solute atoms segregate into interface front. Once the composition of the final solidification reaches the eutectic point, eutectic reaction occurs; or the final solidification zones are cooled below the solidus, the liquid solidifies and solidification finishes. The type and morphology of the as-cast microstructures in the final solidification zones are determined by the concentration of solute atoms in and the size of the zones.

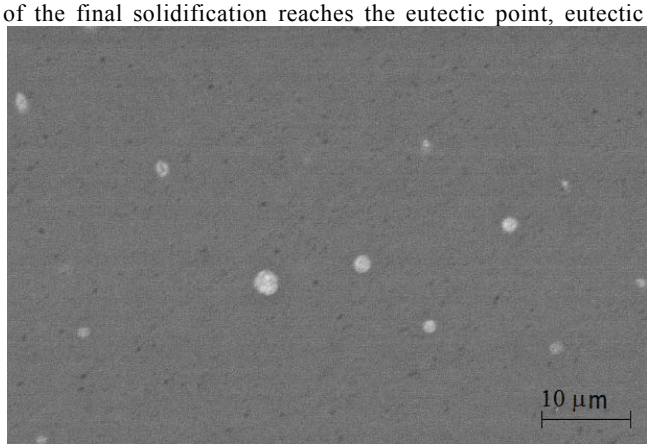

Figure 6 (a) as-cast microstructure of Sample5

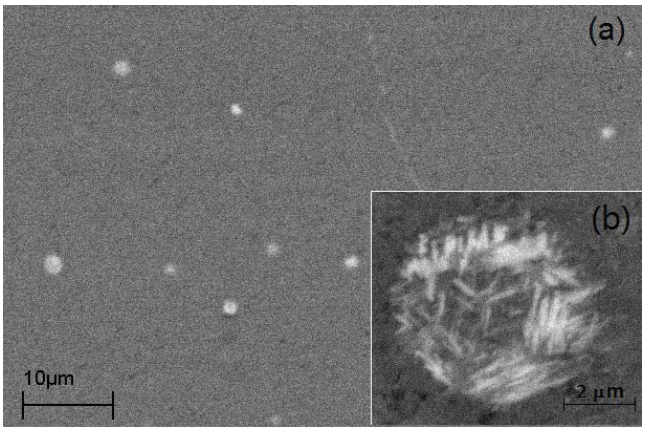

Figure 7 (a) as-cast microstructure of Sample 6 and (b) flake-like structure

Although the content of iron in the alloy is very low, under the condition of slow cooling (Sample 1), the iron segregated into the final solidification zone and formed eutectic compounds. At the triangle grain boundaries, the final solidifications were high in concentration in solute atoms and large in size, which created eutectic compounds Al_3Fe in lamellar or Chinese script morphologies. At the boundaries of two grains, the eutectic compounds Al_tFe were sheet shaped and low in iron content. It is assumed that in the final solidification zone, there are relatively low concentrations of iron between the two grains, and the gap is thin in size.

Increasing cooling rate could result in two impacts on the solidification behavior: minishing grain size and reducing the segregation trend of solute atoms. Both of these factors would give rise to the decrease in the concentration of solute atoms in the final solidification zone. The decrease in the concentration of solute atoms would result in the formation of eutectic compound with lower composition of solute atoms. In Sample 3, no Al_3Fe was observed. The intermetallics were mainly $Al_tFe(Si)$; only a few $Al_mFe(Si)$ phases were formed in some eutectic clusters. It is assumed that $Al_mFe(Si)$ can only formed in the final solidification zones which contain relatively high iron content. In all other zones the concentration of iron is relatively low. With further increase in cooling rate, the final solidification zones contained even less iron, which resulted in the disappearance of $Al_mFe(Si)$ phase in the latter samples.

Reducing the size of the final solidification zone would give rise to the change of the shape of the eutectic clusters. At the triangle grain boundaries, the eutectic clusters changed from triangle form to round form. For example, in Sample 3, which was solidified at a high cooling rate, some eutectic structures at triangle grain boundaries started to round up from one angle; many rounded clusters appeared.

With the increase in cooling rate, the grain decreases in size and increases in number. In return, the final solidification zones in the triangle grain boundaries and inter-dentrites increase in number and decrease in size. Therefore, the eutectic clusters formed in the final solidification zones increase in number and decrease in size. For example, in Sample 5, it was observed that more, but smaller, eutectic clusters were formed than that in the previous samples. However, with the further increase in cooling rate, although the final solidification increased, the concentrations of the solute atoms decreased. In some final zone, the concentrations of the solute atoms were too low to form a eutectic compound. Hence, the amount of the eutectic clusters in Sample 6 decreased.

Conclusions

(1) The as-cast microstructure of Sample 1, which solidified at 0.037°C/s, consisted of primary α-Al dendrites and eutectic compounds Al_tFe and Al_3Fe. The Al_3Fe contained small amount of silicon and formed typical lamellar or Chinese script structures; the Al_tFe was of sheet-like structure and displayed a strip-like morphology at the metallographic face. No significant amount of silicon was detected in the EDX analysis.

(2) The as-cast microstructure changed with the increasing of cooling rate. When the sample solidified at a high cooling rate, eutectic compound changed from Al_3Fe to Al_tFe; Al_3Fe disappeared.

(3) Increasing cooling rate resulted in the decrease of solidification temperature and the appearance of supercooling. When the sample was cooled at a rate of 65°C/s, the solidification temperature was reduced to 645°C; the supercooling was 7.8°C.

(4) Increasing cooling rate promoted the eutectic clusters to change from triangle structure to round form and decrease in both size and number.

Acknowledgements

The authors are grateful to the Research Foundation of Shenyang Aerospace University for its financial support.

References

(1) M. C. Flemings, Solidification Processing at Near-Rapid and Rapid Rates, Weinberg F International Symposium on Solidification Processing, USA, Pergamon Press, 1990, 173-194.

(2) Fu Hengzhi and XieFaqin, Science and Technology of Advanced Materials, 2(2001), 193-196.
(3) David N. Hazelett and Wojtek S. Szczypiorski, Hazelett Process – Smelter Metal to Sheet, Presented at the Guthrie Honorary Symposium, Montreal, Canada, June 7, 2011
(4) L.F. Mondolfo, Aluminium Alloys Structure and Properties, Butter Worths, 1976
(5) C. M. Allen et al, Progress in Materials Science, 43 (1998) 89-170.
(6) Tomasz Stuczynski and Marzena Lech-Grega, Light Metals 2003, Edited by Paul N. Crepeau, 961-968.
(7) Yanhua Zhang et al, Journal of Alloys and Compounds, 473 (2009) 442-445.
(8) D. Panahi et al, Canadian Metallurgical Quarterly, 50 (2011) 173-181.
(9) Per Skjerpe, Metall. Trans. A, 18 (1987) 189-200.
(10) W. Khalifa, F. H. Samuel and J. E. Gruzleski, Metall. Mater. Trans. A, 34 (2003) 807¨C825.
(11) W. Khalifa et al, Metall. Mater. Trans. A 36 (2005) 1017-1032.
(12) Yi Han et al, Materials Transactions, 47(2006)2, 2092-2098
(13) E. J. Westerman, Aluminum Alloys for Packaging, Editted by J. G. Morris et al, 1993, 1-15